

Pollen-Based Magnetic Microrobots are Mediated by Electrostatic Forces to Attract, Manipulate, and Kill Cancer Cells

Carmen C. Mayorga-Martinez, Michaela Fojtů, Jan Vyskočil, Nam-Joon Cho, and Martin Pumera*

AbstractNaturally occurring micro/nanoparticles provide an incredible array of potential sources when preparing hybrid micro/nanorobots and their intrinsic properties can be exploited as multitasking functionalities of modern robotics as well as ensuring their mass production availability. Herein, magnetic biological bots (BioBots) prepared from defatted sunflower pollen microparticles by ferromagnetic metal layer evaporation on one side of its surface are described. It is demonstrated that the methodology employed introduces magnetic properties to sunflower pollen microparticles-based BioBots and enable their magnetic actuation. Interestingly, as-prepared magnetic sunflower pollen-based BioBots can naturally attract cancer cells due to their opposite charges (positive and negative, respectively). Such attracted cancer cells can then be transported by microrobots. This strong attraction also allows the delivery of drugs intended to kill the cancer cells. Sunflower-based BioBots can be fabricated in large quantities, and are naturally programmable, making them promising candidates for cancer cell therapy.

1. Introduction

Magnetic micro/nanorobots are leading the field of micro/nanomotor technology research due to their maneuverability, directional control, programed swarm behavior, and biocompatibility.^[1–7] However, current production methodologies are limited when using magnetic materials at different sizes and shapes such as roll-up technology, 3D laser lithography, template-based approach combined with electrodeposition techniques, and chemical synthesis.^[1,2,8–10]

There is significant interest in using naturally occurring micro/nanomaterials as a source of micro/nanorobots as these materials are in reproducible shapes and available in nature in large quantities.^[11–16] Besides, such materials ensure their abundance to mass produce as micro/nanorobots and also offer biocompatibility.

Plant-based micro/nanorobots, e.g., pollen microparticles,^[17–19] plant tissues,^[20,21] plant cells,^[22] and microalgae,^[23,24] are of particular interest due to their biocompatibility and ability to be easily modified to perform multiple functions.

Particularly, pollen microparticles^[25] represent a very promising naturally available material to be used as a skeleton to fabricate smart microrobots. Since they are abundant in nature, biodegradable,^[26–28] and monodisperse.^[29,30] In addition, pollen microparticle shows enhanced structural stability^[31] thanks to the sporopollenin outer sheath that can even resist the fossilization process. However, the hollow internal shells of pollen microparticles can be used for cargo encapsulation and delivery recently reported by our previous research.^[32–37] Moreover, pollen microparticles have been used as 3D scaffolds,^[38] paper derived from pollen microgels,^[39] pressure sensors,^[40] bio-sensor platform,^[41] flexible pollen-derived substrate for optoelectronic applications,^[42] and water cleaning.^[17,18,43]

On the other hand, pollen microparticles are dynamic entities capable of communicating with other cells by electrostatic forces.^[44] Herein, we take advantage of this capability of sunflower pollen microparticles asymmetrically cover with a ferromagnetic layer to fabricate devices that can attract, manipulate, and kill cancer cells. The obtained magnetic sunflower pollen-based microrobots are referred in the following text as “SFPμP-BioBots.” We have observed that SFPμP-BioBots can naturally


C. C. Mayorga-Martinez, M. Fojtů, J. Vyskočil, M. Pumera
Center for Advanced Functional Nanorobots
Department of Inorganic Chemistry
University of Chemistry and Technology Prague
Technická 5, Prague 166 28, Czech Republic
E-mail: martin.pumera@vscht.cz

M. Fojtů
Department of Pathological Physiology
Faculty of Medicine
Masaryk University
Kamenice 5, Brno 625 00, Czech Republic

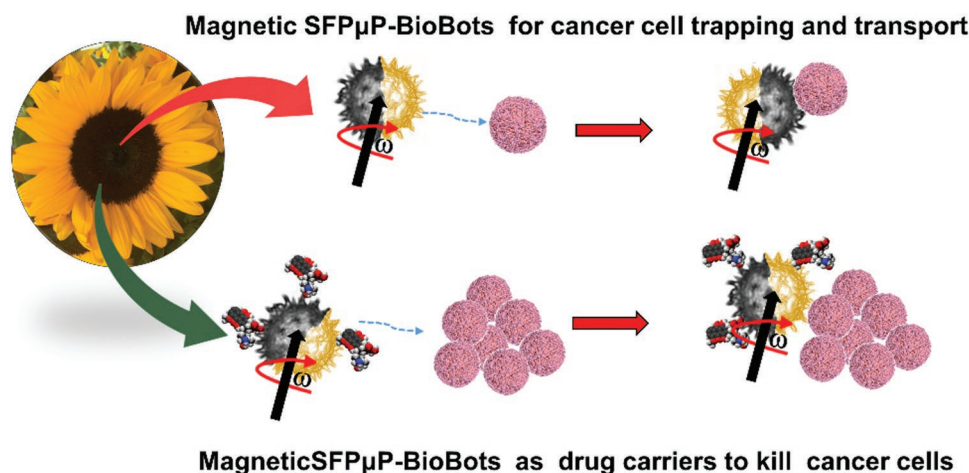
N.-J. Cho
School of Materials Science and Engineering
Nanyang Technological University
50 Nanyang Avenue, Singapore 639798, Singapore

M. Pumera
Faculty of Electrical Engineering and Computer Science
VSB – Technical University of Ostrava
17. listopadu 2172/15, Ostrava 70800, Czech Republic

M. Pumera
Department of Medical Research
China Medical University Hospital
China Medical University
No. 91 Hsueh-Shih Road, Taichung 40402, Taiwan

 The ORCID identification number(s) for the author(s) of this article can be found under <https://doi.org/10.1002/adfm.202207272>.

DOI: 10.1002/adfm.202207272



Scheme 1. Schematic representation of magnetic sunflower pollen-based BioBot (SFPμP-BioBots) interaction with cancer cell. Magnetic SFPμP-BioBots used to attract and transport cancer cells (top panel), and as drug carriers to kill the cancer cells (bottom panel).

attract cancer cells and transport them by a transversal rotating magnetic field. The magnetic element was introduced by asymmetrical deposition of sequential metal evaporation of gold, cobalt, and gold using electron beam evaporation. The fabricated SFPμP-BioBots were capable of moving under a transversal rotating magnetic field (Scheme 1, top panel). We utilized the natural attraction between cancer cells and SFPμP-BioBots loaded with doxorubicin (DOX) to investigate their effect on ovarian cancer cells (Scheme 1, bottom panel).

2. Results and Discussion

Magnetic SFPμP-BioBots are prepared by asymmetric deposition of thin film metal layers (Au, Co, and Au) on one side of defatted sunflower pollen microparticles using electron beam evaporation (Figure 1A, see details in the Experimental Section). To prevent oxidation of the cobalt, it was deposited between two layers of gold.

The raw pollen was processed and defatted by using organic solvents (acetone and diethyl ether) to remove lipid and protein, which is the main allergy-causing components of the pollen. Thus, the pollen-based microrobot used in this paper is non-allergenic, confirmed by the previous paper.^[36] In addition, the defatted process can significantly reduce the immunogenicity of DOX-carrying pollen-based microrobots.

Scanning electron microscopy (SEM) images showing SFPμP-BioBots at different magnification (Figure 1B) reveals that the structural integrity of the sunflower pollen microparticle remains intact after the metal layers deposition. In addition, energy-dispersive X-ray spectroscopy (EDS) analysis of SEM images shows the homogeneous distribution of Au and Co elements on one side of the SFPμP-BioBot (Figure 1C).

After confirming that the asymmetric deposition of the metal layers was successful, we evaluated the magnetic actuation of as-prepared magnetic SFPμP-BioBots under a transversal rotating magnetic field in cell culture media (RPMI-1640). Figure 2A–C shows the precise directional control of magnetic

SFPμP-BioBots by changing the angle of the rotation plane on a 2D surface. As can be seen, linear (Figure 2A), circular (Figure 2B), and undulatory locomotion (Figure 2C) of magnetic SFPμP-BioBots can be recorded. These results also demonstrate the strategy employed to magnetize the sunflower pollen microparticle was sufficient for their magnetic actuation. The velocity dependence of magnetic SFPμP-BioBots with the frequency of the transversal rotating field was also evaluated (Figure 2D; Video S1, Supporting Information). Clearly, the linear dependence is evident ($r = 0.94$) and the step-out frequency in cell culture media of magnetic SFPμP-BioBots was ≈ 2 Hz at 3 mT. Figure 2E shows time-lapse image sequences of one complete near-surface revolution during 3 s using 0.3 Hz (Video S2, Supporting Information), demonstrating that the magnetic SFPμP-BioBots exhibit surface walking motion under a transversal rotating magnetic field.

Next, we studied the ability of SFPμP-BioBots to interact and manipulate human ovarian cancer cells. Interestingly, when magnetic SFPμP-BioBots are in contact with human ovarian cancer cell, they are able to naturally attract and transport them (Video S3, Supporting Information). The attraction and transportation of cancer cells by SFPμP-BioBots is due to electrostatic forces.^[44] The overall negative charge of the cancer cell's surface^[45] can be easily attracted to the SFPμP-BioBots' positive surface charge: $\zeta = +8.14 \pm 0.54$ mV. SFPμP-BioBots surface charge was obtained using Z-potential measurements, see experimental section. The negative surface charge of cancer cells is due to cancer cells have extraordinarily high concentrations of negatively charged glycoproteins on their exterior surface, which act as an electrical shield.^[47] On the other hand, electrostatic interactions involve the attraction of ions, molecules or particles with permanent charges of opposite signs. In this sense, we think that the electrostatic interactions of cancer cells (negative charge) with SFPμP-BioBots (positive charge) are possible because they have opposite charges.

First, the cancer cells are attracted by the SFPμP-BioBot without direct contact and transported over long distances (Video S3, Supporting Information, and Figure 3). After a while, the cancer cells are trapped by the SFPμP-BioBots (Video S4,

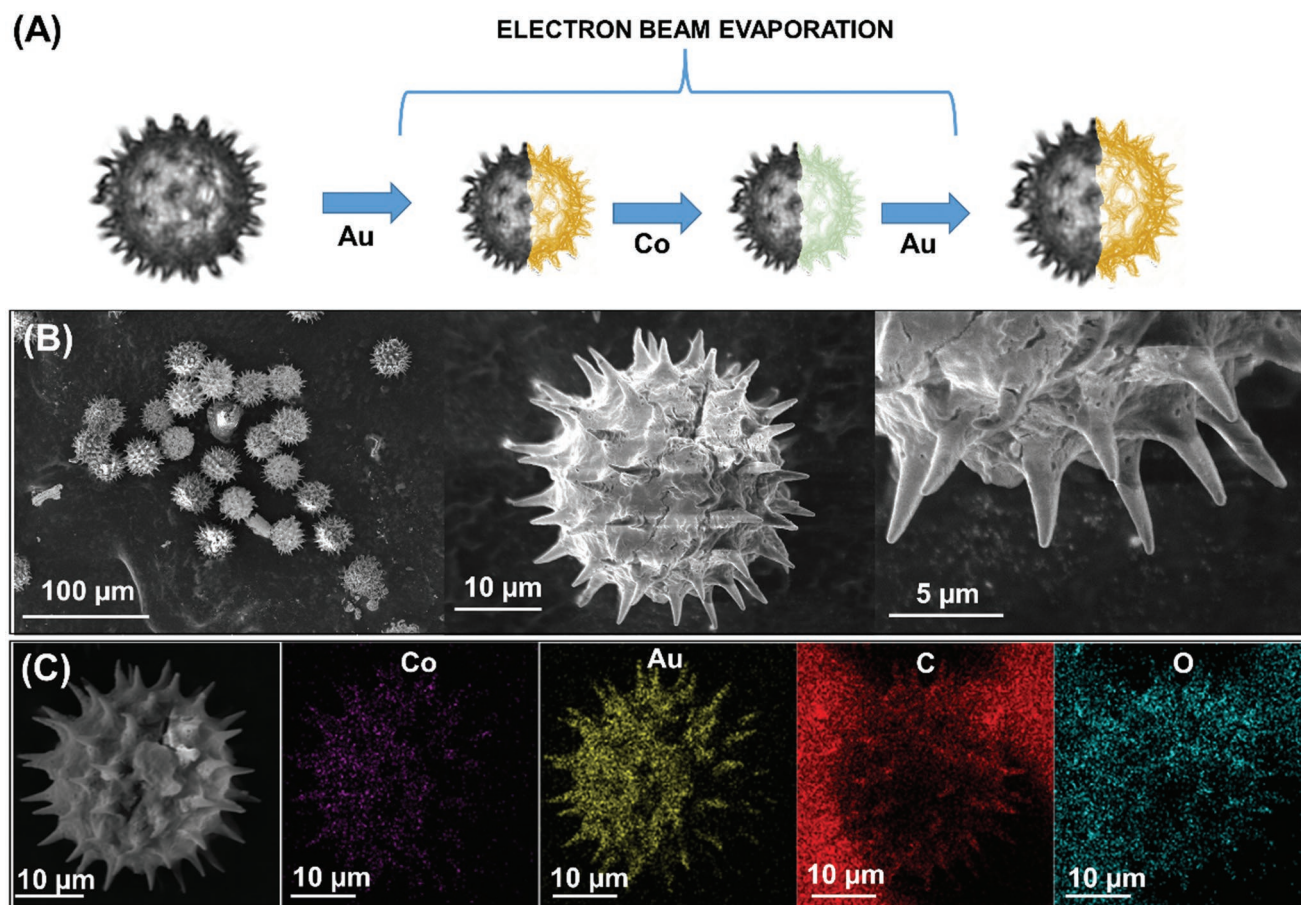


Figure 1. Morphological characterization of magnetic SFP μ P-BioBot. A) Schematic representation of magnetic SFP μ P-BioBot fabrication by asymmetric deposition of Au, Co, and Au on one side of the sunflower pollen microparticle by electron beam evaporation. B) Scanning electron microscopy (SEM) images at different magnifications. C) EDS elemental mapping obtained from SEM images of magnetic SFP μ P-BioBots.

Supporting Information). In addition, magnetic SFP μ P-BioBots can walk freely on the surface of cancer cells seeded on a flat surface as single SFP μ P-BioBots or as doublet or triplet SFP μ P-BioBots (Video S5, Supporting Information). However, after some time, the SFP μ P-BioBots suddenly stops and stick to the surface of the cancer cells (Video S6, Supporting Information).

Due to the strong electrostatic interactions between magnetic SFP μ P-BioBots and cancer cells, DOX was loaded on SFP μ P-BioBots surface and their ability to kill A2780 cells was assessed. Our previous research demonstrated that sunflower pollen microparticles are able to load DOX efficiently and kill human breast cancer cells (MCF-7).^[17] However, these pollen microparticles were used as catalytic micromotors that needed a high concentration of H₂O₂ for propulsion. H₂O₂ is not biocompatible, therefore, these micromotors are used in limit under static mode only (i.e., no H₂O₂).^[17]

To assess the effect of metal layers deposited on one side of SFP μ P-BioBots, we first assessed the DOX binding efficiency of pristine sunflower pollen microparticles in culture medium after 24 h incubation (Figure 4, blue line). DOX was applied in the concentration range of 0–15 $\times 10^{-6}$ M and the concentration of pristine pollen microparticles was 25 μ g mL⁻¹ across the whole DOX concentration range. Pristine pollen microparticles evinced high binding efficiency, ranging 20.6–99.9%

(Table 1). With up to 0.5 $\times 10^{-6}$ M DOX concentration the binding efficiency increased, peaking \approx 99.9%, at higher concentration, the efficiency rapidly decreased. However, in case of SFP μ P-BioBots, the binding efficiency, in general, decreased significantly, ranging 2.4–32.9%. With up to 1 $\times 10^{-6}$ M DOX concentration the binding efficiency increased, peaking \approx 32.9%, and then declined at higher concentrations (Figure 4, red line). Therefore, the surface coating of pollen microparticles with Au, Co, and Au layers reduced the DOX binding efficiency significantly. Further experiments with DOX@SFP μ P-BioBots (magnetic SFP μ P-BioBots bound with DOX) were thus performed to discover whether the binding efficiency, i.e., the amount of DOX carried by SFP μ P-BioBots, is sufficient to induce efficient cancer cell death in ovarian cancer cells. To cargo DOX on SFP μ P-BioBots, we used passive loading. As reported before, DOX were uniformly loaded into the central cavity of pollen grains by passive loading due to eudicots aperture and nano-holes of sunflower pollen.^[36,37] Moreover, a quick release of DOX over the time is expected because of its high water solubility, apertures, and nano-holes of pollen.^[36,37]

The behavior of magnetic SFP μ P-BioBots in a biological system was further assessed as well as their efficacy to deliver a drug (DOX) in a targeted manner and on the therapeutic efficiency of DOX. First, the general toxicity of magnetic

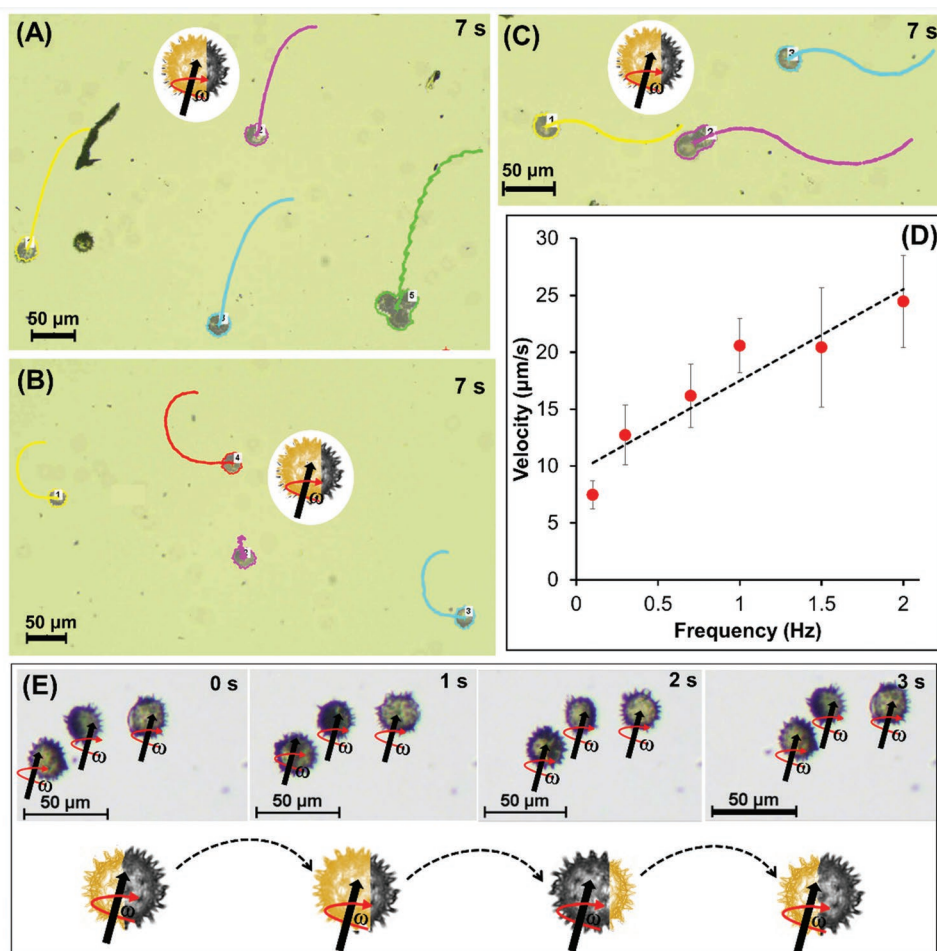


Figure 2. Magnetic actuation of magnetic SFPμP-BioBots. Digital images with tracking lines of linear (A), circular (B), and undulatory (C) trajectories of magnetic SFPμP-BioBots under a transversal rotating magnetic field at 1 Hz. D) Velocity average of SFPμP-BioBots at different rotational frequencies using 3 mT of magnetic field intensity, values are the average of ten independent measurements. Data are displayed as mean ± SD. E) The motion mechanism of the SFPμP-BioBots was evaluated at 0.3 Hz and 3 mT.

SFPμP-BioBots themselves was assessed toward the A2780 cell line. These were applied in concentrations ranging 0–25 μg mL⁻¹ for 24 and 48 h. In the case of 24 h, the SFPμP-BioBots were found to be non-toxic across the whole concentration range, i.e., the viability of A2780 cells did not drop under 80% (ranging 101–80%, see Figure S1 and Table S1, Supporting Information). After 48 h incubation, the viability slightly declined, ranging 100–78%. Therefore, the highest concentration of magnetic SFPμP-BioBots (25 μg mL⁻¹) was safe to use for the drug delivery. For this purpose, two similar experimental setups were established: 25 μg mL⁻¹ of SFPμP-BioBots were incubated with DOX (0–5 × 10⁻⁶ M) differing in the absence/presence of the applied transversal rotating magnetic field, see Figure 5A,B. In addition, an experiment that corresponds to free DOX (0–5 × 10⁻⁶ M) was evaluated as well (see Figure S3, Supporting Information). In the absence of the transversal rotating magnetic field, the A2780 viability gradually declined, dropping to 36.9% when the SFPμP-BioBots with highest DOX concentration (5 × 10⁻⁶ M) was applied. However, when a predefined rectangular trajectory of SFPμP-BioBots under a transversal rotating magnetic field was applied using programmed

automated motion mode^[46] (see Video S7 and Figure S2, Supporting Information), the viability of A2780 cancer cells was reduced even more, dropping to 26.4% with increasing DOX concentration. On the other hand, cell viability was reduced to 32.1% at the highest concentration of free DOX (Figure S3, Supporting Information). The enhancement of DOX anti-cancer activity mediated by SFPμP-BioBots under transversal rotating field was 17.4% ± 3.8, 16.0% ± 18.5, 20.0% ± 16.5, and 6.3% ± 7.6, for 0, 0.5, 1, 5 × 10⁻⁶ M of DOX, respectively. Values are average of three independent measurements (*n* = 3).

3. Conclusions

It is demonstrated here that hybrid biological bots based on pollen microparticles are able to attract, manipulate, and kill ovarian cancer cells. The interaction between SFPμP-BioBots and cancer cells is mediated by electrostatic forces. These electrostatic forces are generated by the negative and positive surface charge of cancer cells and SFPμP-BioBots, respectively. As a result, the strong attraction between them allows the

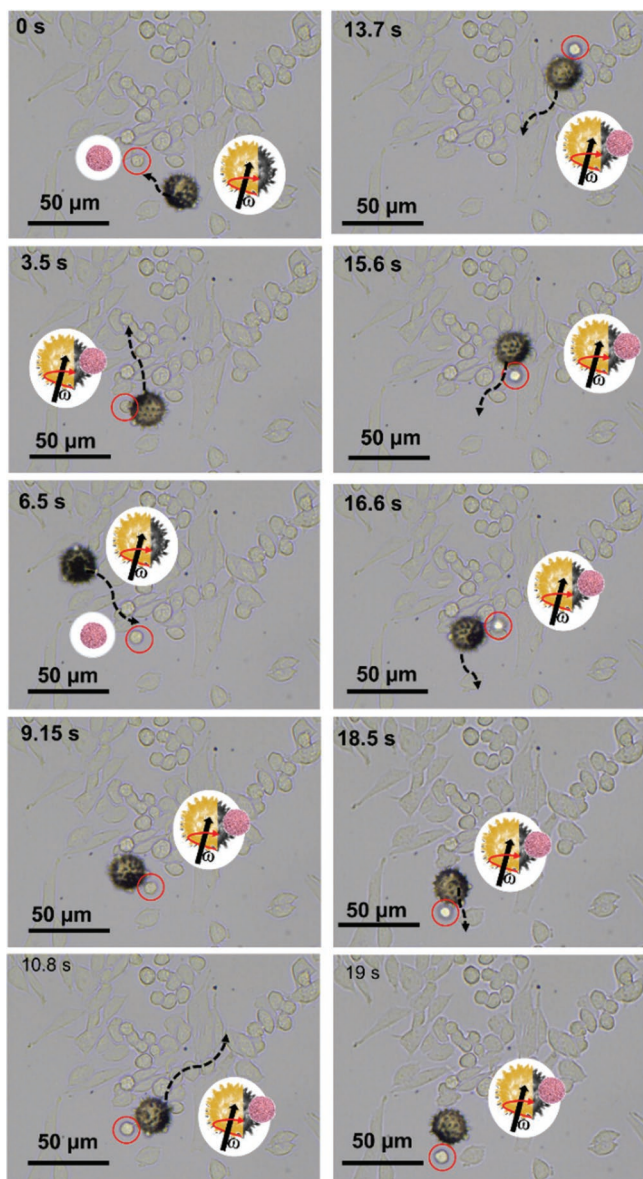


Figure 3. Manipulation of cancer cell by magnetic SFP μ P-BioBots. Time lapse images of magnetic SFP μ P-BioBots attracting and transporting a free cancer cell as well as interaction with seeded cancer cells.

doxorubicin delivery close to the surrounded of cancer cells. To fabricate the magnetic SFP μ P-BioBots, asymmetric ferromagnetic thin layers were deposited on one side of pollen microparticles by e-beam evaporation. This methodology was successful to magnetize pollen microparticles for their magnetic actuation.

Table 1. Doxorubicin binding efficiency: Efficacy of DOX binding (%) on the surface of pristine sunflower pollen microparticles and magnetic SFP μ P-BioBots after their incubation in PBS for 24 h.

	0×10^{-6} M DOX	0.05×10^{-6} M DOX	0.1×10^{-6} M DOX	0.25×10^{-6} M DOX	0.5×10^{-6} M DOX	1×10^{-6} M DOX	5×10^{-6} M DOX	15×10^{-6} M DOX
Pristine pollen microparticles [%]	0.0 ± 0.0	58.6 ± 1.9	71.1 ± 1.1	91.4 ± 2.3	99.9 ± 2.4	94.5 ± 7.9	43.9 ± 2.3	20.6 ± 0.1
Magnetic SFP μ P-BioBots [%]	0.0 ± 0.0	2.4 ± 0.0	9.5 ± 0.1	23.9 ± 1.2	29.0 ± 0.7	32.9 ± 0.4	24.2 ± 1.4	12.4 ± 0.3

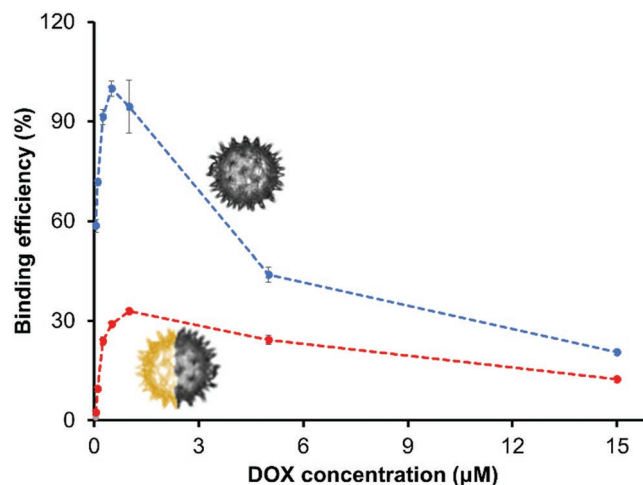


Figure 4. Doxorubicin (DOX) binding efficiency experiments. Pristine pollen microparticles (red line) and magnetic SFP μ P-BioBots (blue line) were incubated with different DOX concentrations in PBS for 24 h. Values are the average of four independent measurements. Data are displayed as mean \pm SD.

In addition, the magnetic field can penetrate human body, so we can still control the pollen-based microrobots to move inside human body.^[2] Moreover, pollen is edible and used in medicinal application.^[47]

4. Experimental Section

Chemical and Biochemical Reagents: Fetal bovine serum (FBS, mycoplasma-free), penicillin, streptomycin, and trypsin were purchased from PAA Laboratories GmbH (Paching, Austria). Doxorubicin solution (2 mg mL^{-1}) was purchased from Teva Pharmaceuticals (Prague, Czech Republic). RPMI-1640 medium, phosphate-buffered saline pH 7.2 (PBS), MTT reagent, ethylenediaminetetraacetic acid (EDTA), dimethyl sulfoxide (DMSO), glycine buffer, and all other chemicals of ACS purity were purchased from Merck (Darmstadt, Germany) unless noted otherwise.

Morphological Characterization of SFP μ P-BioBots: SEM microscopy and elemental mapping of SFP μ P-BioBots were performed using a scanning electron microscope (TESCAN MAIA 3) coupled with an energy-dispersive spectrometer (EDS) (Oxford Instruments, UK). Z-potential measurements (three replicates) were carryout using ZETASIZER PRO (Malvern) with a DTS1070 folded Capillary Zeta Cell (ANAMET s.r.o.).

SFP μ P-BioBots Fabrication: Natural sunflower pollen microparticles were defatted using a methodology reported before.^[17,48–50] For this aim, 250 g of sunflower pollen microparticles were refluxed in 0.5 L of acetone under magnetic stirring at $50 \text{ }^\circ\text{C}$ and 220 rpm for 3 h. After that, acetone was decanted and 1 L of deionized water was added for 1 h. Subsequently, the resulting solution was filtrated through a $300 \text{ }\mu\text{m}$ diameter pore size nylon mesh and $6 \text{ }\mu\text{m}$ diameter pore size filter paper. To hydrate pollen microparticles, 1 L deionized water was added, and

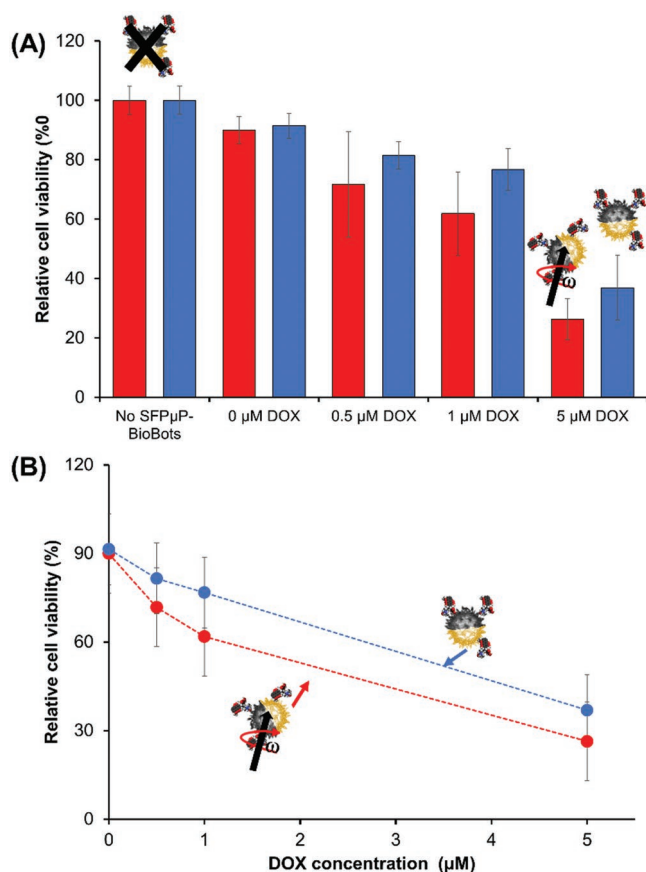


Figure 5. A) Cytotoxicity evaluation to A2780 cell in presence of magnetic DOX@SFPμP-BioBots under transversal magnetic rotating field (red column) and static mode, not transversal magnetic rotating field (blue column). SFPμP-BioBots loaded with different DOX concentration. B) Relative A2780 cell viability as a function of DOX concentration loaded on SFPμP-BioBots in static and dynamic modes. Values are the average of three independent measurements performed in triplicate. Data are displayed as mean ± SD.

magnetic stirring was applied for 30 min and the solution filtered again. Obtained samples, were refluxed again in acetone followed by acetone separation by vacuum filtration and the sample stored in a glass Petri dish in a fume hood for 1 day. Two hundred fifty milliliters of dry pollen samples (20 g) was mixed with diethyl ether and stirred for 120 min (400 rpm, 25 °C), repeating this step twice. After repetition of the last step twice, diethyl ether was removed by vacuum filter. Thereafter, diethyl ether was added to the pollen sample under overnight magnetic stirring. Finally, the sample was separated from diethyl ether by filtering and transferred to a petri dish and left to dry for 12 h in a fume hood.

To obtain the SFPμP-BioBots, a solution containing 5 mg mL⁻¹ of plant-based microcapsules was dropped onto a glass slide and left to dry overnight. After that, 40 nm layers of gold, cobalt, and gold were asymmetrically evaporated onto one side by an e-beam evaporator. Subsequently, the SFPμP-BioBots were removed by mechanical scraping to ensure that the majority of the particles were detached from the glass slide and the powder was collected.

SFPμP-BioBots Propulsion under a Transversal Rotating Magnetic Field: SFPμP-BioBots magnetic propulsion was evaluated in RPMI-1640 medium and a transversal rotating magnetic field was generated by a homemade magnetic field and a 3D-printed six-coil system attached to a microscope table. The magnetic intensity used in all the experiments was 3 mT.^[51]

Cell Line and Cell Culture: The human ovarian cancer cell line A2780 was obtained from the Health Protection Agency Culture Collections (Salisbury, UK). Cells were cultivated in RPMI-1640 medium with 10% FBS and 1% antibiotic supplementation (penicillin 100 U mL⁻¹ and streptomycin 0.1 mg mL⁻¹). The A2780 cells were established from the tumor tissue of an untreated patient with ovarian endometrioid adenocarcinoma. Cells were routinely allowed to grow exponentially while maintained in the incubator at 37 °C in 5% CO₂ mixture with ambient air.

Cytotoxicity of Magnetic SFPμP-BioBots: The A2780 ovarian cancer cells were seeded on 96-well plates at a density of 12 000 cells per well, ensuring 70% confluence on the third day after cell seeding. The cells were grown in a complete RPMI-1640 culture medium and incubated at 37 °C in a humidified 5% CO₂ mixture with ambient air. On the third day of cell incubation, magnetic SFPμP-BioBots were applied (concentration range 0–25 μg mL⁻¹, 200 μL per well). The cells were exposed to the effect of magnetic SFPμP-BioBots for 24 and 48 h. After this, the cell culture media with magnetic SFPμP-BioBots was replaced with fresh culture media containing MTT (1 mg mL⁻¹, 200 μL per well). The plates were wrapped in aluminum foil and kept in the incubator in a humidified atmosphere at 37 °C for 4 h. After that, culture medium containing MTT was discarded and the cells were re-suspended in 99.9% DMSO (200 μL per well) to dissolve the formazan crystals. Then, glycine buffer (25 μL per well) was added to DMSO and the absorbance was read at 570 nm using a Cytation 3 Imaging reader (BioTek Instruments, Winooski, VT, USA). All measurements were performed in tetraplicate. Magnetic SFPμP-BioBots were also tested for their potential interference with MTT assay in terms of contributing to the absorbance signal at a given wavelength and of reducing the MTT themselves. No interference was detected in the PBS or culture medium.

Loading of DOX on Magnetic SFPμP-BioBots: DOX was loaded on the surface of magnetic SFPμP-BioBots. For SFPμP-BioBots-mediated drug targeting, material concentration 25 μg mL⁻¹ was used as it was shown to be non-toxic (viability > 80%) toward A2780 cells in a previous experiment. SFPμP-BioBots were incubated with an increasing concentration of DOX ranging from 0 to 15 × 10⁻⁶ M in PBS for 24 h. Samples were then centrifuged twice (2 °C, 9000 rpm, 60 min) and washed with PBS. After the last centrifugation, the DOX@sunflower pollen microparticles and DOX@SFPμP-BioBots samples were re-suspended in culture medium according to the requirements of the individual experiment.

DOX Binding Efficiency of SFPμP-BioBots: Sunflower pollen microparticles and SFPμP-BioBots (25 μg mL⁻¹) were incubated with an increasing concentration of DOX (0–15 × 10⁻⁶ M) in culture medium for 24 h. The binding efficiency (BE) was then determined by measuring the fluorescence in the supernatant of these samples. After removing the particles by centrifugation (2 °C, 9000 rpm, 60 min), DOX fluorescence in the supernatants was detected by a Cytation 3 Imaging reader using a 580 nm bandpass emission filter and excitation 475 nm (BioTek Instruments, Winooski, VT, USA). The percentage of DOX bound onto the surface of particles, i.e., the BE was determined by relating it to the data acquired by fluorescence measurement (475 nm excitation, 580 nm emission) of the free DOX at the same concentration range in RPMI 1640 culture medium using the same spectrophotometer. The drug BE was calculated using Equation (1):

$$BEx (\%) = 100 - \left(100 \times \frac{A_{\text{particles@DOX}x}}{A_{\text{DOX}x}} - \left(100 \times \frac{A_{\text{particles}}}{A_0} - 100 \right) \right) \quad (1)$$

where *BEx* is a binding efficacy for selected concentration *x*, *A_{particles@DOX_x}* represents the absorbance of the supernatant obtained after the centrifugation of sunflower pollen microparticles or SFPμP-BioBots with DOX at concentration *x* and *A_{DOX_x}* represents the absorbance of the DOX solution at the same concentration *x*, *A_{particles}* represents the absorbance of the supernatant obtained after the centrifugation of sunflower pollen microparticles or SFPμP-BioBots without DOX and *A₀* represents the absorbance of PBS without any

treatment or particles applied. For the calculation of BE in PBS, a calibration curve of DOX in PBS was used. For the calculation of DOX BE in cell culture medium, a calibration curve of DOX in the cell culture medium was used.

DOX Effectivity using Magnetic SFPμP-BioBots: After proving successful and efficient DOX binding on the surface of SFPμP-BioBots, an evaluation of their ability to target anticancer therapy toward the A2780 cells was conducted. The A2780 cells were seeded on 24-well plates (70 000 cells per well). Magnetic pollen microrobots (25 μg mL⁻¹) were incubated with increasing concentration of DOX (0–5 × 10⁻⁶M) in PBS for 24 h (conditions found to ensure the highest BE) while constantly agitated. After incubation, DOX@SFPμP-BioBots (i.e., magnetic SFPμP-BioBots loaded with DOX) were washed three times with PBS and centrifuged (2 °C, 9000 rpm, 60 min) to remove unbound drug. Then, DOX@SFPμP-BioBots were re-suspended in a complete RPMI 1640 medium and added to the cells. Two identical experimental setups were established, differing only in the presence or absence of a predefined rectangular trajectory of DOX@SFPμP-BioBots under a transversal rotating magnetic field using programmed automated motion mode (3 mT, 2 Hz, 30 min).^[48] The plates were then incubated at 37 °C in a humidified CO₂ atmosphere for 24 h. After this, the effect of DOX@SFPμP-BioBots treatment and the effect of magnetic guidance on cell viability were assessed by removing the old media and replacing it with fresh media containing MTT reagent (1 mg mL⁻¹). Plates with culture medium containing MTT were incubated at 37 °C in a humidified CO₂ atmosphere for 4 h wrapped in aluminum foil. Then, the medium containing MTT was removed and the cells resuspended in 99.9% DMSO (200 μL per well) containing glycine buffer (25 μL per well) to dissolve formazan crystals formed from MTT by cellular oxidoreductases. The absorbance was read at a wavelength of 570 nm. The relative cell viability percentage was calculated using Equation (2):

$$\text{Relative cell viability (\%)} = 100 \times \frac{A_x}{A_0} \quad (2)$$

where A_x represents the absorbance of supernatant for investigated condition and A_0 represents the absorbance of cells without any treatment or particles applied.

Statistical Analysis: For velocity performance evaluation (Figure 2D), the velocity of ten SFPμP-BioBots at different frequencies ($n = 10$) were carried out. The doxorubicin binding efficiency experiments, values are the average of three independent measurements. For cytotoxicity evaluation to A2780 cell (Figure 5; Figures S1 and S3, Supporting Information), values were the average of three independent measurements performed in triplicate. In all cases, data were displayed as mean ± standard deviation (SD) and processed using microsoft excel software.

Supporting Information

Supporting Information is available from the Wiley Online Library or from the author.

Acknowledgements

This work was supported by the project “Advanced Functional Nanorobots” (reg. No. CZ.02.1.01/0.0/0.0/15_003/0000444 financed by the EFRR), the Ministry of Health of the Czech Republic (NU21-08-00407), and Ministry of Education, Youth and Sports (Czech Republic) grant LL2002 under ERC CZ program.

Conflict of Interest

The authors declare no conflict of interest.

Authors Contribution

C.C.M.M. and M.P. devised the project. C.C.M.M. prepared SFPμP-BioBots and characterized their morphological structure, evaluated the magnetic actuation of SFPμP-BioBots, recorded and processed videos, carried out the formal analysis and wrote the original draft. M.F. carried out the DOX-loading and cell viability experiments and helped to write the original manuscript. J. V. designed and constructed the magnetic control setup. N.-J. C. prepared the defeated sun flower pollen microparticles. M.P. initiated and oversaw the project. All authors contributed to writing the paper.

Data Availability Statement

The data that support the findings of this study are available from the corresponding author upon reasonable request.

Keywords

biological microrobots, drug deliveries, hybrid robotics, magnetic micromotors

Received: June 26, 2022

Revised: August 12, 2022

Published online:

- [1] X.-Z. Chen, M. Hoop, F. Mushtaq, E. Siringil, C. Hu, B. J. Nelson, S. Pané, *Appl. Mater. Today* **2017**, *9*, 48.
- [2] H. Zhou, C. C. Mayorga-Martinez, S. Pané, L. Zhang, M. Pumera, *Chem. Rev.* **2021**, *121*, 4999.
- [3] C. C. J. Alcântara, F. C. Landers, S. Kim, C. De Marco, D. Ahmed, B. J. Nelson, S. Pané, *Nat. Commun.* **2020**, *11*, 5957.
- [4] F. Mushtaq, X.-Z. Chen, H. Torlakcik, B. J. Nelson, S. Pané, *Nano Res.* **2020**, *13*, 2183.
- [5] D. Jin, K. Yuan, X. Du, Q. Wang, S. Wang, L. Zhang, *Adv. Sci.* **2021**, *33*, 2100070.
- [6] B. Wang, K. F. Chan, K. Yuan, Q. Wang, X. Xia, L. Yang, H. Ko, Y.-X. Wang, J. J. Y. Sung, P. W. Y. Chiu, *L. Zhang Sci. Robot.* **2021**, *6*, eabd2813.
- [7] J. Li, T. Li, T. Xu, M. Kiristi, W. Liu, Z. Wu, J. Wang, *Nano Lett.* **2015**, *15*, 4814.
- [8] C. C. J. Alcântara, F. C. Landers, S. Kim, C. De Marco, D. Ahmed, B. J. Nelson, S. Pané, *Nat. Commun.* **2020**, *11*, 5957.
- [9] J. Wu, B. Jang, Y. Harduf, Z. Chapnik, Ö. B. Avci, X. Chen, J. Puigmartí-Luis, O. Ergeneman, B. J. Nelson, Y. Or, *S. Pané Adv. Sci.* **2021**, *8*, 2004458.
- [10] M. Guix, C. C. Mayorga-Martinez, A. Merkoçi, *Chem. Rev.* **2014**, *114*, 6285.
- [11] J. G. S. Moo, C. C. Mayorga-Martinez, H. Wang, B. Khezri, W. Z. Teo, M. Pumera, *Adv. Funct. Mater.* **2017**, *27*, 1604759.
- [12] A. A. Solovev, Y. Mei, E. B. Ureña, ; G. Huang, O. G. Schmidt, *Small* **2009**, *5*, 1692.
- [13] H. Wang, M. Pumera, *Adv. Funct. Mater.* **2018**, *28*, 170542.
- [14] X. Liang, L. Li, J. Tang, M. Komiyama, K. Ariga, *Bull. Chem. Soc. Jpn* **2020**, *93*, 581.
- [15] M. Urso, M. Pumera, *Adv. Funct. Mater.* **2022**, 2200711.
- [16] E. Del Grosso, E. Franco, L. J. Prins, F. Ricci, *Nat. Chem.* **2022**, *14*, 600.
- [17] T. Maric, M. Z. M. Nasir, N. F. Rosli, M. Budanović, R. D. Webster, N.-J. Cho, M. Pumera, *Adv. Funct. Mater.* **2020**, *30*, 2000112.

- [18] H. Wang, M. G. Potroz, J. A. Jackman, B. Khezri, T. Marić, N. J. Cho, M. Pumera, *Adv. Funct. Mater.* **2017**, *27*, 1702338.
- [19] M. Sun, K. F. Chan, Z. Zhang, L. Wang, Q. Wang, S. Yang, S. Melissa Chan, P. W. Y. Chiu, J. J. Y. Sung, L. Zhang, *Adv. Mater.* **2022**, 2201888.
- [20] W. Gao, X. Feng, A. Pei, C. R. Kane, R. Tam, C. Hennessy, J. Wang, *Nano Lett.* **2014**, *14*, 305.
- [21] H. Wang, J. Guo, S. Moo Pumera, *M. Nanoscale* **2014**, *6*, 11359.
- [22] D. Huska, C. C. Mayorga-Martinez, R. Zelinka, M. Pumera, *Small* **2022**, *18*, 2200208.
- [23] F. Zhang, Z. Li, L. Yin, Q. Zhang, N. Askarinam, R. Mundaca-Urbe, F. Tehrani, E. Karshalev, W. Gao, L. Zhang, J. ang, *J. Am. Chem. Soc.* **2021**, *143*, 12194.
- [24] D. Gong, J. Cai, N. Celi, L. Feng, Y. Jiang, D. Zhang, *J. Magn. Magn. Mater.* **2018**, *468*, 148.
- [25] Q. Shi, M. S. B. Ibrahim, X. Zhang, Y. Hwang, H. Chin, S. Chen, W. S. Tan, H. Li, J. Song, N.-J. Cho, *Appl. Mater. Today* **2022**, *27*, 101471.
- [26] E.-L. Tan, M. G. Potroz, G. Ferracci, L. Wang, J. A. Jackman, N.-J. Cho, *Appl. Mater. Today* **2020**, *18*, 100525.
- [27] T.-F. Fan, M. G. Potroz, E.-L. Tan, M. S. Ibrahim, E. Miyako, N.-J. Cho, *Sci. Rep.* **2019**, *9*, 9626.
- [28] T.-F. Fan, M. G. Potroz, E.-L. Tan, J. H. Park, E. Miyako, N.-J. Cho, *Sci. Rep.* **2019**, *9*, 2944.
- [29] J. Seo, L. Wang, W. Ng, N.-J. Cho, *ChemNanoMat* **2016**, *2*, 414.
- [30] E.-L. Tan, M. G. Potroz, G. Ferracci, J. A. Jackman, H. Jung, L. Wang, N.-J. Cho, *Adv. Funct. Mater.* **2018**, *28*, 1707568.
- [31] T.-F. Fan, M. G. Potroz, E.-L. Tan, M. S. Ibrahim, E. Miyako, N.-J. Cho, *Sci. Rep.* **2019**, *9*, 9626.
- [32] A. K. Prabhakar, M. G. Potroz, E.-L. Tan, H. Jung, J. H. Park, N.-J. Cho, *ACS Appl. Mater. Interfaces* **2018**, *10*, 28428.
- [33] M. G. Potroz, R. C. Mundargi, J. J. Gillissen, E.-L. Tan, S. Meker, J. H. Park, H. Jung, S. Park, D. Cho, S.-I. Bang, N.-J. Cho, *Adv. Funct. Mater.* **2017**, *27*, 1700270.
- [34] R. C. Mundargi, M. G. Potroz, S. Park, J. H. Park, H. Shirahama, J. H. Lee, J. Seo, N.-J. Cho, *Adv. Funct. Mater.* **2016**, *26*, 487.
- [35] R. C. Mundargi, E.-L. Tan, J. Seo, N.-J. Cho, *J. Ind. Eng. Chem.* **2016**, *36*, 102.
- [36] R. C. Mundargi, M. G. Potroz, S. Park, H. Shirahama, J. H. Lee, J. Seo, N.-J. Cho, *Small* **2016**, *12*, 1167.
- [37] A. K. Prabhakar, M. G. Potroz, S. Park, E. Miyako, N.-J. Cho, *Part. Syst. Character.* **2018**, *35*, 1800151.
- [38] S. Chen, Q. Shi, T. Jang, M. S. B. Ibrahim, J. Deng, G. Ferracci, W. S. Tan, N.-J. Cho, J. Song, *Adv. Funct. Mater.* **2021**, *31*, 2106276.
- [39] Z. Zhao, Y. Hwang, Y. Yang, T. Fan, J. Song, S. Suresh, N.-J. Cho, *Proc. Natl. Acad. Sci. USA* **2020**, *117*, 8711.
- [40] L. Wang, J. A. Jackman, E.-L. Tan, J. H. Park, M. G. Potroz, E. T. Hwang, N.-J. Cho, *Nano Energy* **2017**, *36*, 38.
- [41] L. Wang, W. Ng, J. A. Jackman, N.-J. Cho, *Adv. Funct. Mater.* **2016**, *26*, 2097.
- [42] Y. Hwang, A. Sadhu, S. Shin, S. W. Leow, Z. Zhao, J. Deng, J. A. Jackman, M. Kim, L. H. Wong, N.-J. Cho, *Adv. Mater.* **2021**, *33*, 2100566.
- [43] Y. Hwang, M. S. B. Ibrahim, J. Deng, J. A. Jackman, N.-J. Cho, *Adv. Funct. Mater.* **2021**, *31*, 2101091.
- [44] Y. Vaknin, S. Gan-Mor, A. Bechar, B. Ronen, D. Eisikowitch, *Plant Syst. Evol.* **2000**, *222*, 133.
- [45] Z. Li, J. Ruan, X. Zhuang, *J. Nanobiotechnol.* **2019**, *17*, 59.
- [46] C. C. Mayorga-Martinez, J. Vyskočil, F. Novotný, P. Bednar, D. Ruzek, O. Alduhaishe, M. Pumera, *Appl. Mater. Today* **2022**, *26*, 101337.
- [47] H. F. Linskens, in *Fertilization in Higher Plants* (Eds: M. Cresti, G. Cai, A. Moscatelli), Springer, Berlin, Heidelberg, Germany **1999**, 27.
- [48] T.-F. Fan, S. Park, Q. Shi, X. Zhang, Q. Liu, Y. Song, H. Chin, M. S. B. Ibrahim, N. Mokrzecka, Y. Yang, H. Li, J. Song, S. Suresh, N.-J. Cho, *Nat. Commun.* **2020**, *11*, 1449.
- [49] Z. Zhao, J. Kumar, Y. Hwang, J. Deng, M. S. B. Ibrahim, C. Huang, S. Suresh, N.-J. Cho, *Proc. Natl. Acad. Sci. U.S.A.* **2021**, *118*, e2113715118.
- [50] Z. Zhao, J. Deng, H. Tae, M. S. Ibrahim, S. Suresh, N.-J. Cho, *Adv. Mater.* **2022**, *34*, 2109367.
- [51] J. Vyskočil, C. C. Mayorga-Martinez, E. Jablonská, F. Novotný, T. Ruml, M. Pumera, *ACS Nano* **2020**, *14*, 8247.